Small-angle x-ray transition radiation from multilayered structures

A. A. Savchenko,[1,2] D. Yu. Sergeeva,[1,2] A. A. Tishchenko,[1,2,*] and M. N. Strikhanov[1]
[1]National Research Nuclear University "MEPhI", Moscow 115409, Russian Federation
[2]National Research Center "Kurchatov Institute," Moscow 123098, Russian Federation

(Received 12 July 2018; published 25 January 2019)

In this work, we construct for the first time the theory of small-angle transition radiation from multilayered structures. The theoretically obtained spectral and angular distributions of radiated photons are compared with those predicted by GEANT4, a very popular package used today for numerical simulation of different physical processes. We demonstrate that, while spectral distributions ideally coincide, the angular ones differ. We argue that transition radiation from the multilayered structure must contain sharp spikes having the interference nature and caused by the effect of merging two maximum frequencies in dispersive media, and thus GEANT4 needs improving in this respect. The transition radiation theory developed here for the small-angle case can play a vital part for the possible future Small Angle Spectrometer at the LHC, other experiments of this kind, and detectors for hadrons of the tera-electron-volt energy range.

DOI: 10.1103/PhysRevD.99.016015

I. INTRODUCTION

Various cosmic-ray experiments and experiments on modern and future accelerators face the challenge to identify particles with Lorentz factors up to $\sim 10^5$. For example, widely used transition radiation detectors are good for the separation of electrons from the hadron background up to hadron Lorentz factors of about 500. For a higher Lorentz factor, the contribution of transition radiation from hadrons becomes significant and almost reaches saturation at Lorentz factors of about 3×10^3. The identification of charged particles of ultrahigh energies, therefore, is an extremely difficult task, and now there are no detectors capable of identifying the single charged particles with reliable efficiency in this range of Lorentz factors. One of the examples in which such a type of detectors should play a crucial role is the study of hadron production within small angles at the Large Hadron Collider [1]. This experiment requires the separation of protons, K mesons, and pi mesons in the energy range of 1–6 TeV. Besides measurement of fundamental QCD processes defining particles production with low transverse momentum at LHC energies, these experiments are extremely important for astroparticle physics. Such experiments will allow us to resolve ambiguities related to the models of particle production at energies up to 10^{17} eV in the Universe, in which the particle spectrum is observed to change significantly. Therefore, existing transition radiation-based detectors and trackers need further development.

Transition radiation (TR) is emitted when a charged particle crosses the boundary between two different media. Since TR was theoretically predicted by Ginzburg and Frank in 1945 [2], there have been many works dedicated to different aspects of this type of radiation, but x-ray TR became especially useful due to its applications for detecting high-energy particles [3–7]. Today, TR is widely used in different experiments at accelerators in so-called transition radiation detectors (TRD) or trackers (TRT) [8–10], for example, TRT in ATLAS or TRD in ALICE (LHC, CERN), CBM (FAIR), etc.

While TR theory is well developed for relatively simple cases, the radiative processes in real radiators include many different phenomena following TR. Therefore, nowadays, in detector physics, it is conventional to use the powerful instruments of computer modeling.

One of the most advanced and popular instruments is Geant, which has been developing since 1974 at CERN and other leading scientific centers. The latest version of Geant is GEANT4 [11]; since being issued quite recently, in 2006, it has already become the leading toolkit for computer simulations in different branches of nuclear and radiation physics, such as accelerator physics [12–14], physics of high energy [15–21], medical physics [22,23], space studies [24,25], etc. Also, it is the fourth version of Geant in which the x-ray TR module was incorporated for the first time.

While the GEANT4 x-ray TR module is based on the well-known theory of Garibian adapted by Grichine and others [26–29], it exploits a fast simulation (parametrization) approach developed for the description of electromagnetic showers [30]. It is caused by the fact that at the

*alexey.tishchenko@cern.ch

creation of this TR module for GEANT4 there were theoretical spectral-angular and spectral distributions, but there were no analytical expression for angular distribution. It is natural, therefore, that the x-ray TR module of GEANT4 is not a mere repetition of the Garibian's theory but, in a way, is some new predicting instrument differing from the pure theory. Along with that, accurate calculation of angular distributions can be indispensable for new TR detectors valid for the precise detection of hadrons in the tera-electron-volt range. This paper aims to develop well-established theoretical models of TR for the case of angular distribution of small-angle radiation.

The paper is organized as follows. In Sec. II A, we describe the existing background in the theory of TR. In Sec. II B, we derive analytically the angular distribution of x-ray TR from a multilayered structure. Section III contains the short explanation about GEANT4, and then in Sec. IV, we perform a cross-model comparison between theoretical expressions obtained here and GEANT4 simulation results. In Sec. V, we discuss the key features of angular distribution of x-ray TR. Section VI supplements the theoretical results of Sec. II B with the role of the air between films, which makes the theory be closer to the experimental reality. In the concluding section, Sec. VII, we sum up the results of this research.

II. THEORETICAL MODELS OF TR

Among a plenty of theoretical research devoted to TR, we choose probably the two most elaborated models proposed by G. M. Garibian [31–33] and by V. E. Pafomov [34–36]. To avoid encumbering the text, we will not go into the details of similarities and differences between these two theories. There is, however, one issue worth mentioning here. Equation (22.10) in the widely known paper by Pafomov [34] contains the misprint: the wrong $e^{-i\psi}$ in $f(\omega,\theta)$ instead of the correct $e^{-i\varphi}$, which is given in Eq. (1) of his earlier paper [35] and also in [36], being the Springer edition of Ref. [34]. As, except for this misprint, both theories demonstrate perfect coincidence of spectral-angular distributions, and the Garibian's one is more convenient to deal with in terms of analytics, below we shall use the Garibian's theory..

Let us consider x-ray TR generated from the regular radiator; see Fig. 1(a).

A. Spectral-angular and spectral distributions

The expression for spectral-angular distribution of x-ray TR at $\theta \ll 1$ according to Garibian has the form (Eq. (3.15) in Ref. [33]),

$$\frac{d^2W_G(\omega,\theta)}{d\theta d\omega} = \frac{e^2}{c}\frac{\omega^2\theta^3}{8\pi c^2}|Z_m - Z_{\rm vac}|^2\left[(1-Q^{1/2})^2 + 4Q^{1/2}\sin^2\left(\mathrm{Re}\frac{a}{Z_m}\right)\right]F_M(\omega,\theta), \tag{1}$$

where $Z_{\rm vac}$ and Z_m are the formation zones in vacuum and in media:

$$Z_{\rm vac} = \frac{4c}{\omega(\gamma^{-2}+\theta^2)}, \qquad Z_m = \frac{4c}{\omega(\gamma^{-2}+\theta^2+1-\varepsilon(\omega))}, \tag{2}$$

$$F_M(\omega,\theta) = \frac{(1-Q^{M/2})^2 + 4Q^{M/2}\sin^2\left(M\mathrm{Re}\left(\frac{a}{Z_m}+\frac{b}{Z_{\rm vac}}\right)\right)}{(1-Q^{1/2})^2 + 4Q^{1/2}\sin^2\left(\mathrm{Re}\left(\frac{a}{Z_m}+\frac{b}{Z_{\rm vac}}\right)\right)},$$
$$Q = \exp\left[-\frac{\omega a\varepsilon''(\omega)}{c}\right]. \tag{3}$$

Here, γ is the Lorentz factor; M is the number of films in the stack; a and b are thicknesses of films and gaps, respectively; and ε is the permittivity of radiator material,

$$\varepsilon = \varepsilon(\omega) = \varepsilon'(\omega) + i\varepsilon''(\omega) = 1 - \frac{\omega_0^2}{\omega^2} + \frac{i\nu(\omega)c}{\omega}, \tag{4}$$

with ω_0 being the plasma frequency of radiator material (we used $\omega_0 = 20.871$ eV for polypropylene) (see, e.g., Ref. [5]), $\nu(\omega)$ being the linear absorption coefficient, which can be defined using the data from Ref. [37]. The imaginary part of permittivity $\varepsilon''(\omega)$ is responsible for absorption of TR in radiator material. Here, we have taken into account that $d\Omega = \sin\theta d\theta d\phi$ and have integrated over $d\phi$.

Though the dielectric function given by Eq. (4) has a universal asymptotic form, this form can change in the very narrow spectral regions near the lines of characteristic radiation, where the real part of dielectric susceptibility

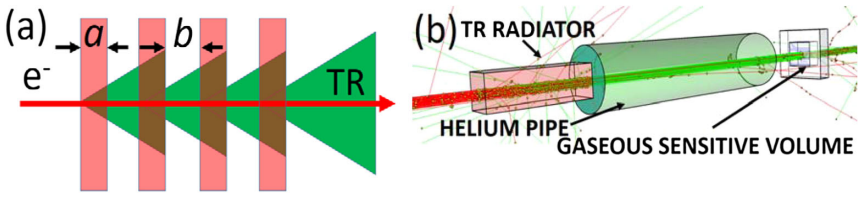

FIG. 1. (a) Scheme of radiator generating TR. The radiator is a multilayered structure consisting of M films with the width a (pink) and vacuum (or air) gaps of the width b between them. Green areas symbolize TR. (b) GEANT4 visualization of TR detector. Red tracks are charged particles, and green tracks are x-ray TR photons or other neutral particles.

$[\varepsilon'(\omega)-1]$ changes its sign. Because of that, for example, x-ray Cherenkov radiation can occur in where $\varepsilon'(\omega)>0$ (see, e.g., Ref. [38]) or, in the crystals, where the dynamic scattering of radiation can lead to the effective condition like $\varepsilon'_{\rm eff}(\omega)>0$, so that parametric x-ray radiation can take place [39]. Though the explicit form of the dielectric function can play a part in the calculations similar to those from Sec. II B, discussion of these questions would go beyond the scope of this research devoted to the conventional transition radiation.

As for the spectral distributions of TR, according to Garibian, it has the form (Eq. (3.31) in Ref. [33]):

$$\frac{dW_G(\omega)}{d\omega}=\frac{e^2\omega M_{\rm eff}}{4c^2(a+b)}\sum_{n=1,2,3...}\theta_n^2|Z_{\rm vac}-Z_m|^2\times\left((1-Q^{1/2})^2+4Q^{1/2}\sin^2\left[{\rm Re}\frac{a}{Z_m}\right]\right)\Big|_{\theta=\theta_n}, \tag{5}$$

$$M_{\rm eff}=\frac{1-Q^M}{1-Q},\qquad \theta_n^2=\frac{4\pi c(n-d)}{\omega(a+b)},\qquad d=C-{\rm floor}(C), \tag{6}$$

$$C=\frac{\omega(a+b)}{4\pi c}\left[(1-\varepsilon')\frac{a}{a+b}+\gamma^{-2}\right]. \tag{7}$$

Here, floor (C) means the largest integer not exceeding C. Equation (5) is the result of integrating Eq. (1) over all values of θ when $M\gg 1$.

For further comparison of theoretical models with GEANT4 simulation, one has to operate with the values $dN/d(\hbar\omega)$ and $dN/d\theta$, which are connected with the theoretical formulas given above as

$$\frac{dN}{d(\hbar\omega)}=\frac{1}{\omega\hbar^2}\frac{dW(\omega)}{d\omega}=\frac{1}{\omega\hbar^2}\int d\theta\frac{d^2W(\theta,\ \omega)}{d\theta d\omega}, \tag{8}$$

$$\frac{dN}{d\theta}=\int d\omega\frac{1}{\omega\hbar}\frac{d^2W(\theta,\ \omega)}{d\theta d\omega}, \tag{9}$$

where N is the number of radiated photons.

B. Angular distribution of x-ray transition radiation from multiple stack of films: Exact calculation

As for the angular distributions of TR, for $Q=1$ and $M\gg 1$, we have

$$F_M(\omega,\theta)|_{Q=1}=\frac{\sin^2\left(M{\rm Re}\left(\frac{a}{Z_m}+\frac{b}{Z_{\rm vac}}\right)\right)}{\sin^2\left({\rm Re}\left(\frac{a}{Z_m}+\frac{b}{Z_{\rm vac}}\right)\right)}\xrightarrow{M\gg 1}\pi M\sum_r\delta\left({\rm Re}\left(\frac{a}{Z_m}+\frac{b}{Z_{\rm vac}}\right)-\pi r\right). \tag{10}$$

The result of integration of Eq. (1) over all considered frequencies

$$\omega_{\rm min}\le\omega\le\omega_{\rm max} \tag{11}$$

can be written in the form

$$\frac{dN(\theta)}{d\theta}=\frac{1}{137}\frac{\theta^3M}{2c^2}\sum_{r=r_{1,\rm min}}^{r_{1,\rm max}}|Z_m-Z_{\rm vac}|^2\sin^2\left({\rm Re}\frac{a}{Z_m}\right)\frac{\omega_1^3}{|A\omega_1^2-B|}\Big|_{\omega=\omega_1}+\frac{1}{137}\frac{\theta^3M}{2c^2}\sum_{r=r_{2,\rm min}}^{r_{2,\rm max}}|Z_m-Z_{\rm vac}|^2\sin^2\left({\rm Re}\frac{a}{Z_m}\right)\frac{\omega_2^3}{|A\omega_2^2-B|}\Big|_{\omega=\omega_2}, \tag{12}$$

where

$$A=(a+b)(\theta^2+\gamma^{-2})/4c, \tag{13}$$

$$B=a\omega_0^2/4c, \tag{14}$$

and the frequencies

$$\omega_{1,2}=\frac{\pi r\pm\sqrt{(\pi r)^2-4AB}}{2A} \tag{15}$$

should satisfy the inequality in Eq. (11).

To find $r_{1,\rm max}$, $r_{1,\rm min}$, $r_{2,\rm max}$, and $r_{2,\rm min}$, the following analysis should be performed. Let us designate

$$\begin{aligned}A_1&=2\sqrt{AB}/\pi,\\ A_2&=2A\omega_{\rm max}/\pi,\\ A_3&=(A\omega_{\rm max}^2+B)/\pi\omega_{\rm max},\\ A_4&=2A\omega_{\rm min}/\pi,\\ A_5&=(A\omega_{\rm min}^2+B)/\pi\omega_{\rm min}.\end{aligned} \tag{16}$$

Solving the inequality

$$\omega_{\rm min}\le\omega_1\le\omega_{\rm max}, \tag{17}$$

we obtain the systems

$$\begin{cases} r \geq A_1, A_4, \\ r \leq A_2, A_3, \end{cases} \text{ or } \begin{cases} r \geq A_1, A_5, \\ r \leq A_3, A_4, \end{cases} \tag{18}$$

from which, assuming that r is a positive integer number, one can find that if $A_1 \leq A_2$, A_3 and $A_4 \leq A_3$ then

$$\text{ceiling}(\max\{A_1, A_4\}) \leq r \leq \text{floor}(\min\{A_2, A_3\}) \tag{19}$$

or if $A_1 \leq A_3$, A_4 and $A_5 \leq A_3$, A_4 then

$$\text{ceiling}(\max\{A_1, A_5\}) \leq r \leq \text{floor}(\min\{A_3, A_4\}), \tag{20}$$

otherwise, the first sum in Eq. (12) does not contain any summand. Here, ceiling(x) means the smallest integer exceeding x.

In its turn, the inequality

$$\omega_{\min} \leq \omega_2 \leq \omega_{\max} \tag{21}$$

is fulfilled if at least one of two systems are correct,

$$\begin{cases} r \geq A_1, A_4, \\ r \leq A_2, A_5, \end{cases} \text{ or } \begin{cases} r \geq A_1, A_2, A_3, \\ r \leq A_5, \end{cases} \tag{22}$$

from which one can find that if $A_4 \leq A_5$ and $A_1 \leq A_2$, A_5 then

$$\text{ceiling}(\max\{A_1, A_4\}) \leq r \leq \text{floor}(\min\{A_2, A_5\}), \tag{23}$$

or if $A_5 \geq A_1$, A_2, A_3 and $A_5 \leq A_3$, A_4 then

$$\text{ceiling}(\max\{A_1, A_2, A_3\}) \leq r \leq \text{floor}(A_5), \tag{24}$$

otherwise, the second sum in Eq. (12) does not contain any summand.

Note that the ranges of r given in Eqs. (19) and (20) can overlap, so it is important not to include the same summands in the first sum in Eq. (12). The same is true for Eqs. (23) and (24).

What is interesting, is that if the factor $F_M(\omega, \theta)$ in Eq. (1) represents the set of narrow sharp peaks while all the rest factors are just slowly changing functions of frequency, then it is possible to take into account the photon absorption following the way of calculatings in Ref. [33]. As the result of that instead of Eq. (12) we have

$$\frac{dN(\theta)}{d\theta} = \frac{1}{137}\frac{\theta^3}{8c^2}\sum_{r=r_{1,\min}}^{r_{1,\max}} M_{\text{eff}}|Z_m - Z_{\text{vac}}|^2\left((1-Q^{1/2})^2 + 4Q^{1/2}\sin^2\left[\text{Re}\frac{a}{Z_m}\right]\right)\frac{\omega_1^3}{|A\omega_1^2 - B|}\Bigg|_{\omega=\omega_1}$$
$$+ \frac{1}{137}\frac{\theta^3}{8c^2}\sum_{r=r_{2,\min}}^{r_{2,\max}} M_{\text{eff}}|Z_m - Z_{\text{vac}}|^2\left((1-Q^{1/2})^2 + 4Q^{1/2}\sin^2\left[\text{Re}\frac{a}{Z_m}\right]\right)\frac{\omega_2^3}{|A\omega_2^2 - B|}\Bigg|_{\omega=\omega_2}. \tag{25}$$

Numerical integration of the spectral-angular distribution in Eq. (1) shows very good agreement with Eq. (25), so the latter can be used for further analysis.

III. GEANT4 SIMULATION OF TRANSITION RADIATION

GEANT4 allows obtaining the mean number of x-ray TR photons as well as their energy and emitting angle inside the radiator. The radiator used in GEANT4 is very general; it consists of films separated by gas gaps with fluctuating thicknesses. The TR module was included in GEANT4 by Grichine and the other toolkit developers [26–29].

We performed simulations of the TR detector presented in Fig. 1(b). Primary particles cross the x-ray TR radiator and then after that, along with x-ray TR photons, cross the 2 m helium pipe and the gaseous detector; see Fig. 1(b). The radiator consists of 150 polypropylene foils with density 0.92 g/cm^3 and thickness 62 μm each, separated by 2 mm vacuum gaps.

In Figs. 2(a) and 2(b), one can see typical GEANT4 spectral and angular distributions of TR for different energies of primary particles: electrons (el) and muons (mu). For the reconstruction of the angular distribution, the photon angle relative to the primary particle direction at the exit of radiator is calculated. Here, $dN/d(\hbar\omega)$ is the number of photons per photon energy, and $dN/d\theta$ is the number of photons per angle.

In Fig. 2(b), the curve describing angular distribution of 2 GeV electrons is considerably wider than others. At that, though the Lorentz factors for 2 GeV electrons and for 300 GeV muons are very close, their angular distributions differ. That is because the 2 GeV electrons are subject to relatively large multiple scattering, which makes the angular distribution wider. The scattering for the muons, as much heavier particles, and higher-energy electrons is suppressed.

Though GEANT4 can give the spectrum registered by sensitive volume [see Fig. 1(b)], in order to compare the results with the theoretical ones we shall use GEANT4 simulations of the photon spectrum right after the radiator.

Note that for GEANT4 simulations the absorption being mentioned can be understood as absorption of i) radiated photons (in the material of the films of which the radiator consists) and ii) scattered primary particles. In this paper, speaking of absorption, we mean only the former.

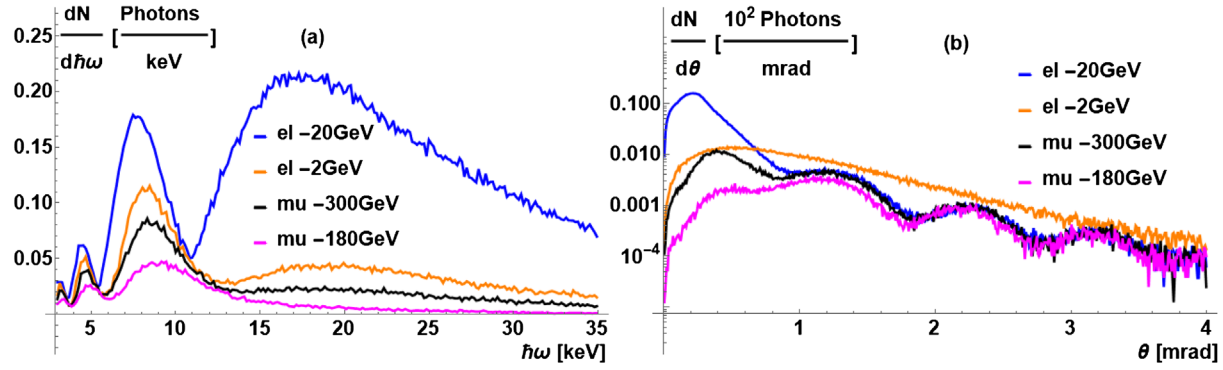

FIG. 2. GEANT4 simulation of (a) spectral and (b) angular distribution of x-ray TR photons after the radiator. The absorption inside the TR radiator is included.

IV. CROSS-MODEL COMPARISON

Figure 3 demonstrates the results of GEANT4 simulation compared with the theoretical TR spectral distributions [parts (a) and (c)] and angular distributions [parts (b) and (d)] for electrons with energies 20 and 2 GeV. The black curves correspond to the theory from Eqs. (5) and (12). We see that i) GEANT4 spectral distribution coincides with the theoretical one both qualitatively and quantitatively and ii) GEANT4 angular distribution drastically differs from that predicted by the theory.

In Fig. 4(a), one can see the dependence, on the photons' energy, of the imaginary part of the permittivity of polypropylene taken as material for the TR radiator. Figures 4(a) and 4(b) show that the absorption affects the radiation distribution mainly at low frequencies (up to 10 keV). It is natural then that Fig. 4(c) shows that the absorption affects the radiation angular distribution mainly at large angles.

V. DISCUSSION OF THE ANGULAR DISTRIBUTIONS

As we see from Figs. 3(b) and 3(d), theory predicts the distinct spikes in angular distribution of TR. Let us explore in more detail from where the spikes come.

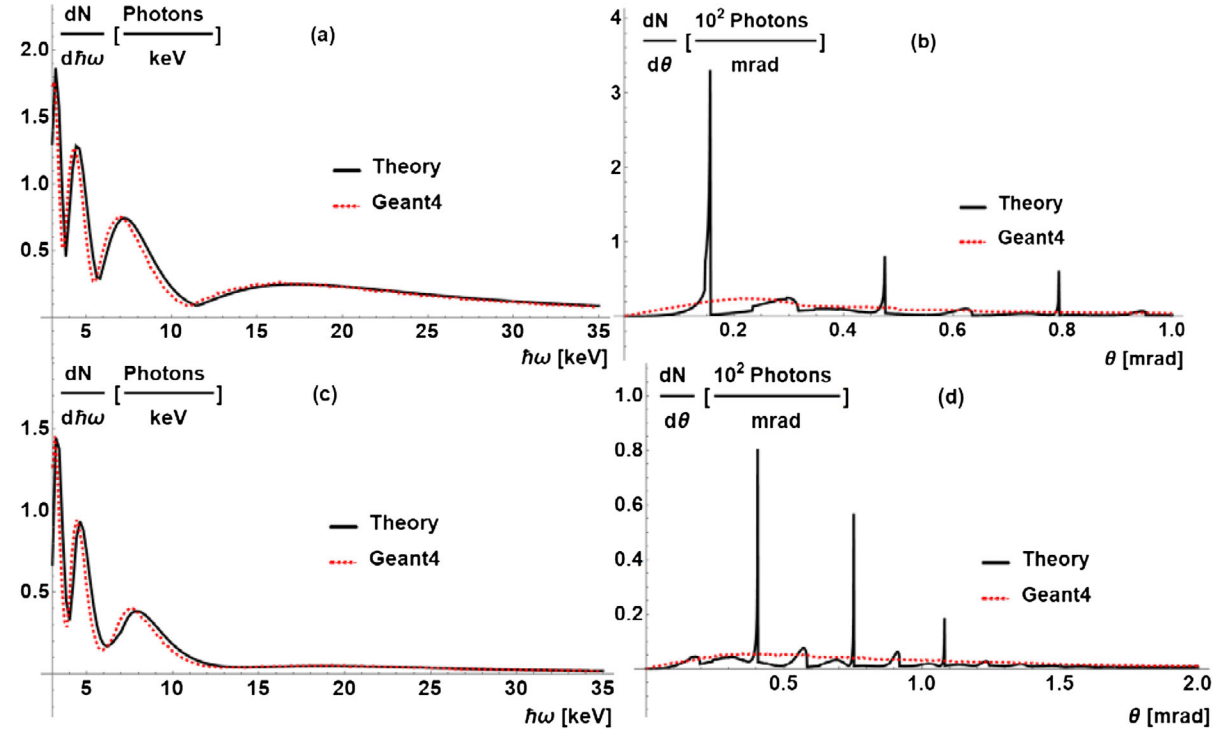

FIG. 3. Comparison of theoretical spectral and angular distributions of x-ray TR photons with GEANT4 simulation results for different energies of electrons crossing TR radiator. Spectral distributions: (a)−20 GeV, (c)−2 GeV. Angular distributions: (b)−20 GeV, (d)−2 GeV.

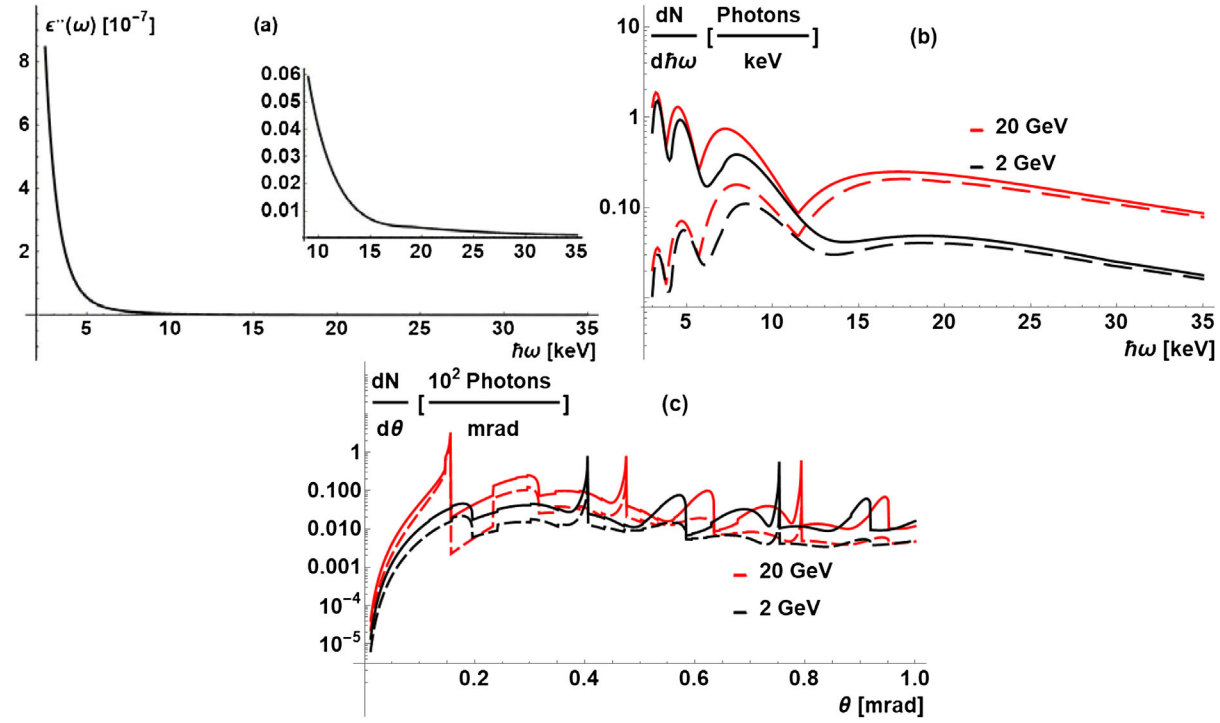

FIG. 4. (a) Dependence of imaginary part of permittivity of polypropylene TR radiator material on the photons energy. (b) Theoretical spectral and (c) angular TR distributions without (solid curves) and with (dashed curves) taking into account absorption of TR photons inside the radiator material.

First, note that the dielectric function in the x-ray and gamma frequency domains has a universal form given by Eq. (4) and does not contain any singularities.

Second, let us look at the dispersion relation of x-ray transition radiation originating from an argument of delta function in Eq. (10):

$$a\omega\left(\gamma^{-2}+\theta^2+\frac{\omega_0^2}{\omega^2}\right)+b\omega(\gamma^{-2}+\theta^2)=4\pi cr. \tag{26}$$

This dispersion relation physically is the result of a complex pattern due to interference of the waves emitted by the periodic structure of radiator.

Resolving this equation relative to the frequency ω, we find the values ω_1 and ω_2 defined by Eq. (15). It means that, at given r, there are two waves at frequencies ω_1 and ω_2 propagating under the same angle θ. Note that frequencies ω_1 and ω_2 are distinct, generally speaking. The fact that we have two frequencies is caused by the frequency dispersion of permittivity $\varepsilon(\omega)=1-\omega_0^2/\omega^2$. The similar effect is known in physics: it is a complex Doppler effect in dispersive media, when several waves with different wavelengths can be emitted under the same angle (see, e.g., Ref. [40]).

We would like to stress that, in talking here about these two frequencies, we mean the maxima of the distribution over the frequencies; of course, there are also photons radiated at frequencies close to these two.

In the variety of angles θ, satisfying the dispersion relation given by Eq. (26), the angles θ^*

$$\theta^*=\sqrt{\frac{4\pi^2c^2r^2}{a\omega_0^2(a+b)}-\gamma^{-2}} \tag{27}$$

are special; waves radiated under these angles have the coinciding frequency $\omega_1=\omega_2$:

$$\omega^*=\frac{a\omega_0^2}{2\pi cr}. \tag{28}$$

The effect of the maximum frequencies merging can be traced in Fig. 5. The red curves in Fig. 5 demonstrate the case in which the radiations with two different wavelengths (photon energy), corresponding to the same diffraction order r, propagate in the same direction. The black curves correspond to the case in which $\omega_1=\omega_2$.

We see that two narrow spectral lines turn into a rather wide single line in the case in which $\omega_1=\omega_2$. Therefore, for transition radiation from a stack of films, this effect, along with the interference of radiation in periodic media, can give the spikes in angular distribution of radiation at the angles defined by Eq. (27).

Actually, the angular distribution in Eq. (12) is proportional to

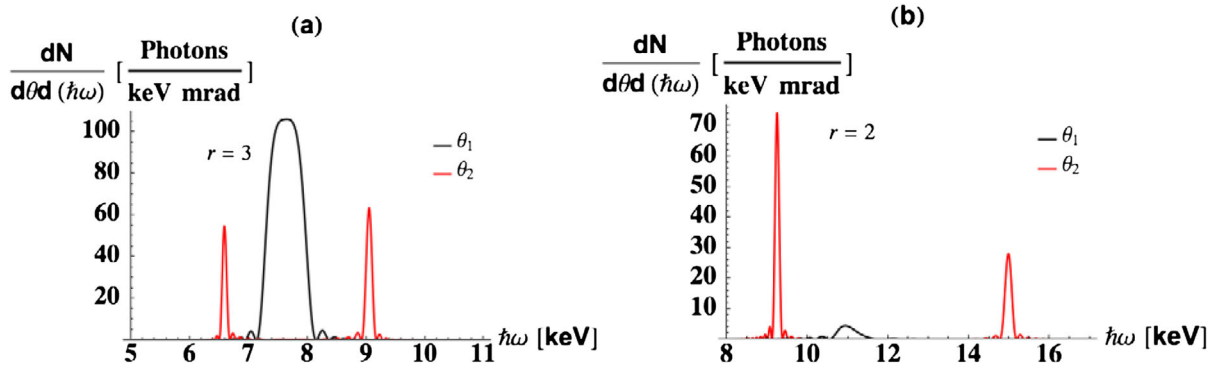

FIG. 5. The distribution of the number of x-ray TR photons per unit angle and per unit photon energy plotted according to Eq. (1) (with no absorption, i.e., $Q = 1$) for fixed angle θ: (a) the third diffraction order ($r = 3$), $\theta_1 = \theta^* = 0.48$ mrad (black curve), $\theta_2 = 0.47$ mrad (red curve); (b) the second diffraction order ($r = 2$), $\theta_1 = \theta^* = 0.32$ (black curve), $\theta_2 = 0.31$ mrad (red curve). All other parameters for all the curves are the same: the electron energy is 20 GeV, and the radiator consists of 150 polypropylene foils with thickness $a = 62$ μm with 2 mm gaps between them.

$$\left.\frac{\omega_{1,2}^3}{|A\omega_{1,2}^2 - B|}\right|_{\omega=\omega_{1,2}}, \tag{29}$$

which is maximal when $\theta = \theta^*$. It is easy to check that the positions of the spikes in Figs. 3(b) and 3(d) are described by Eq. (27) precisely, with the corresponding choice of r.

It is interesting to note that the peaks defined by the denominators in Eq. (29) come from the Dirac delta function of a complex argument [see Eq. (10)]. When the integrals are calculated, these denominators appear because of the corresponding Jacobian factor. Therefore, the resulting resonances are close in their nature and form to the so-called Jacobian peaks known in the particle physics (see, e.g., Ref. [41]).

In Fig. 5, the height of the black maxima depends on the diffraction order r; compare Figs. 5(a) and 5(b). The suppression of the black line in Fig. 5(b) is caused by the influence of the squared sine in Eq. (1) that is responsible for the interference of radiation from two sides of a single film. It explains also why only some of the peaks in Figs. 3(b) and 3(d) have the form of spikes, while the others are suppressed and smoothed.

We can conclude from the said above that physical nature of the spikes is the interference of radiation waves from a set of regular films, at the angles where the two maximum frequencies merge.

The presence of the peaks in angular distribution of x-ray TR was observed experimentally in Ref. [42] for 0.5 GeV electrons, and the peak's positions are perfectly described by Eq. (27).

With respect to the question of why GEANT4, so good in other relations, fails to show the correct angular behavior at small angles, we can just make the cautious assumptions. It is possible that just the accuracy of the calculations within the method implemented in GEANT4 is not high enough. The source of the problem can also lie in the fact that the developers of the toolkit, not having the exact analytical expressions for angular distribution, extracted information about angular distribution from the spectral one [29].

Yet, we would like to stress that these reasons are no more than our assumptions, while to have a complete understanding of all the details of such a versatile and complex package as GEANT4 is a prerogative of the designers. We can just state the fact that GEANT4's frequency distributions perfectly coincide with the theory, while GEANT4's angular distributions repeat the correct behavior at large enough angles but fail to reproduce the sharp peaks at the small ones.

VI. ROLE OF THE AIR BETWEEN FILMS

All formulas given above describe the radiator consisting of material-vacuum layers, while real radiators consist of material-air layers.

For TR generated by ultrarelativistic electrons, the formation zone in air ($\omega_{\rm air}$ is the plasma frequency in air) is

$$Z_{\rm air} = \frac{4c}{\omega(\gamma^{-2} + \theta^2 + 1 - \varepsilon_{\rm air}(\omega))}. \tag{30}$$

For the electrons with the energy 20 GeV, it differs from that in vacuum $Z_{\rm vac}$ when $\omega < 28$ keV, which accounts for the difference between curves in Fig. 6. This difference can affect the radiation spectrum even though $\omega_{\rm air}$ is relatively small (about 0.7 eV). For the dependences and parameters considered, however, this difference proves to be insignificant. Figure 6 shows that the spectral and angular TR distributions coincide with good accuracy for the air and vacuum gaps.

To sum up, the role of air between films can be taken into account as follows:

(1) The spectral-angular distribution is described by Eq. (1) with replacement $Z_{\rm vac}$ by $Z_{\rm air}$.

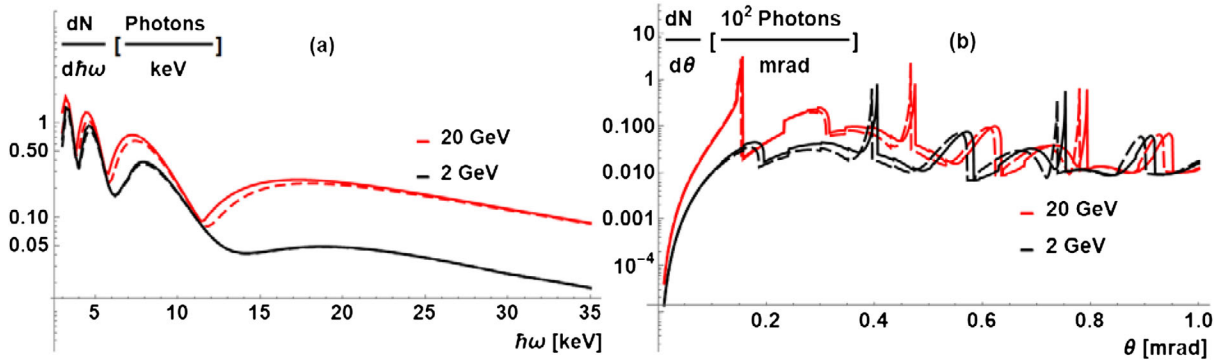

FIG. 6. The comparison of theoretical spectral (a) and angular (b) TR distributions with air (dashed curves) and with vacuum (solid curves) between radiator foils. Here, $\varepsilon'' = 0$, $\varepsilon''_{\text{air}} = 0$.

(2) The spectral distribution (i.e., the spectral-angular one integrated over angles), given by Eq. (5), will remain the same but for two substitutions: i) replacing Z_{vac} by Z_{air} given by Eq. (30) and ii) C from Eq. (7) should be replaced by

$$C_{\text{air}} = \frac{\omega(a+b)}{4\pi c}\left[\frac{a(1-\varepsilon') + b(1-\varepsilon'_{\text{air}})}{a+b} + \gamma^{-2}\right]. \tag{31}$$

(3) The expression describing the spikes' angular position, given by Eq. (27), should be replaced by

$$\theta^*_{\text{air}} = \sqrt{\frac{4\pi^2 c^2 r^2}{(a\omega_0^2 + b\omega_{\text{air}}^2)(a+b)} - \gamma^{-2}}, \tag{32}$$

and, similarly, instead of Eq. (28), we have

$$\omega^*_{\text{air}} = \frac{a\omega_0^2 + b\omega_{\text{air}}^2}{2\pi c r}. \tag{33}$$

(4) The angular distribution (i.e., the spectral-angular one integrated over frequencies) given by Eq. (12) or (25) will equally remain the same but for two substitutions: i) replacing Z_{vac} by Z_{air} given by Eq. (30) and ii) B from Eq. (14) should be replaced by

$$B_{\text{air}} = \omega^2(a(1-\varepsilon') + b(1-\varepsilon'_{\text{air}}))/4c. \tag{34}$$

VII. CONCLUSION

In this work, we developed the theory of x-ray transition radiation from multilayered structure for the case of small angles and compared the theory predictions for spectral and angular distributions of radiated photons with those given by GEANT4.

Figure 3 shows practically ideal agreement between GEANT4 and theoretical spectral distributions and at the same time reveals significant discrepancies between the angular ones, manifested mainly at small angles $\gamma^{-1} < \theta \ll 1$. The spikes occur at the angles defined by Eq. (27) and take place when two maximum frequencies, radiated under the same angle, merge into one.

From the point of view of theory construction, it is interesting that in a similar radiation mechanism, Smith-Purcell radiation, there are no spikes in angular distribution at all. The key difference here consists in the permittivity in the dispersion relation (26) for x-ray TR from periodical structure, unlike the dispersion relation for Smith-Purcell radiation in which no permittivity is contained [43]. It is the frequency dependence of permittivity that changes the behavior of angular distribution of TR so drastically, and the spikes in angular distribution of radiation are defined by the effect of enhancing the radiation when two different frequencies merge, as is demonstrated in Fig. 5.

Thus, the model of angular distribution of x-ray TR incorporated in GEANT4 needs improving. Section II B together with supplementary Sec. V contains all analytical expressions needed for this. The transition radiation theory developed here for the small-angle case can play a vital part for the possible future Small Angle Spectrometer at LHC and other experiments of this kind and, we hope, can play a vital part for developing the detectors capable of detecting ultrarelativistic charged particles with Lorentz factors from 5×10^3 and above, including hadrons of the tera-electron-volt energy range.

ACKNOWLEDGMENTS

The authors would like to thank A. S. Romaniouk, M. G. Albrow, M. L. Cherry, V. O. Tikhomirov, E. J. Schioppa, S. Yu. Smirnov, M. N. Mazziotta, P. Spinelli, F. Loparco, N. Belyaev, E. Shulga, Yu. S. Smirnov, B. L. Bergmann, E. Heijne, and F. Dachs for stimulating discussions. This work was supported by the Russian Science Foundation under Grant No. 16-12-10277.

[1] Small Angle Spectrometer at LHC, https://indico.cern.ch/event/435373/.

[2] V. L. Ginzburg and I. M. Frank, Radiation from a uniformly moving electron due to its transition from one medium into another, Zh. Eksp. Teor. Fiz. **16**, 15 (1946)[J. Phys. USSR **9**, 353 (1945)].

[3] M. L. Cherry, G. Hartmann, D. Muller, and T. A. Prince, Transition radiation from relativistic electrons in periodic radiators, Phys. Rev. D **10**, 3594 (1974).

[4] M. L. Cherry, Measurements of the spectrum and energy dependence of x-ray transition radiation, Phys. Rev. D **17**, 2245 (1978).

[5] B. Dolgoshein, Transition radiation detectors, Nucl. Instrum. Methods Phys. Res., Sect. A **326**, 434 (1993).

[6] P. Nevski, Advances in the simulation of transition radiation detectors, Nucl. Instrum. Methods Phys. Res., Sect. A **522**, 116 (2004).

[7] X. Artru, G. B. Yodh, and G. Mennessier, Practical theory of the multilayered transition radiation detector, Phys. Rev. D **12**, 1289 (1975).

[8] E. Abat *et al.* (ATLAS TRT Collaboration), The ATLAS TRT Barrel Detector, J. Instrum. **3**, (2008).

[9] G. Aad *et al.* (ATLAS Collaboration), The ATLAS experiment at the CERN Large Hadron Collider, J. Instrum. **3**, S08003 (2008); see p. 68.

[10] K. Aamodt *et al.* (ALICE Collaboration), The ALICE experiment at the CERN LHC, J. Instrum. **3**, S08002 (2008); see p. 66.

[11] GEANT4, version 10.4, official web-sites, http://Geant4.web.cern.ch/Geant4/.

[12] D. D. DiJulio, C. P. Cooper-Jensen, H. Björgvinsdóttir, Z. Kokai, and P. M. Bentley, High-energy in-beam neutron measurements of metal-based shielding for accelerator-driven spallation neutron sources, Phys. Rev. ST Accel. Beams **19**, 053501 (2016).

[13] H. N. Tran, M. Karamitros, and V. N. Ivanchenko, GEANT4 Monte Carlo simulation of absorbed dose and radiolysis yields enhancement from a gold nanoparticle under MeV proton irradiation, Nucl. Instrum. Methods Phys. Res., Sect. B **373**, 126 (2016).

[14] G. Alexander, J. Barley, Y. Batygin *et al.*, Observation of Polarized Positrons from an Undulator-Based Source, Phys. Rev. Lett. **100**, 210801 (2008).

[15] U. Husemann, J. Mechnich, and A. Salzburger, Simulation strategies using FATRAS and GEANT4 for a future upgrade of the ATLAS tracking, *J. Phys.* 331, 032046 (2011).

[16] D. Costanzo, A. Dell'Acqua, M. Gallas *et al.*, *The GEANT4-Based Simulation Software of the ATLAS Detector, IEEE Nuclear Science Symposium Conference Record, San Diego, CA, 2006* (IEEE, New York, 2006).

[17] G. Aad *et al.* (ATLAS Collaboration), The ATLAS simulation infrastructure, Eur. Phys. J. C **70**, 823 (2010).

[18] K. Abdel-Waged, N. Felemban, and V. V. Uzhinskii, GEANT4 hadronic cascade models analysis of proton and charged pion transverse momentum spectra from $p + Cu$ and Pb collisions at 3, 8, and 15 GeV/c, Phys. Rev. C **84**, 014905 (2011).

[19] Y. Takubo, R. N. Hodgkinson, K. Ikematsu, K. Fujii, N. Okada, and H. Yamamoto, Measuring anomalous couplings in $H \to WW^*$ decays at the International Linear Collider, Phys. Rev. D **88**, 013010 (2013).

[20] I. Agapov, H. Burkhardt, D. Schulte, A. Latina, G. A. Blair, S. Malton, and J. Resta-López, Tracking studies of the Compact Linear Collider collimation system, Phys. Rev. ST Accel. Beams **12**, 081001 (2009).

[21] F. Berg, L. Desorgher, A. Fuchs, W. Hajdas, Z. Hodge, P. R. Kettle, A. Knecht, R. Lüscher, A. Papa, G. Rutar, and M. Wohlmuther, Target studies for surface muon production, Phys. Rev. ST Accel. Beams **19**, 024701 (2016).

[22] S. Incerti, M. Douglass, S. Penfold, S. Guatelli, and E. Bezak, Review of GEANT4-DNA applications for micro and nanoscale simulations, Phys. Med. **32**, 1187 (2016).

[23] M. B. Hahn, S. Meyer, H.-J. Kunte, T. Solomun, and H. Sturm, Measurements and simulations of microscopic damage to DNA in water by 30 keV electrons: A general approach applicable to other radiation sources and biological targets, Phys. Rev. E **95**, 052419 (2017).

[24] K. Murase, K. Ioka, S. Nagataki, and T. Nakamura, High-energy cosmic-ray nuclei from high- and low-luminosity gamma-ray bursts and implications for multimessenger astronomy, Phys. Rev. D **78**, 023005 (2008).

[25] S. Abe *et al.* (KamLAND Collaboration), Production of radioactive isotopes through cosmic muon spallation in KamLAND, Phys. Rev. C **81**, 025807 (2010).

[26] J. Apostolakis, S. Giani, M. Maire, A. V. Bagulya, and V. M. Grichine, Parameterization models for X-ray transition radiation in the GEANT4 package, Comput. Phys. Commun. **132**, 241 (2000).

[27] V. M. Grichine, Generation of X-ray transition radiation inside complex radiators, Phys. Lett. B **525**, 225 (2002).

[28] V. M. Grichine and S. S. Sadilov, GEANT4 models for X-ray transition radiation, Nucl. Instrum. Methods Phys. Res., Sect. A **522**, 122 (2004).

[29] V. M. Grichine, Angular distribution of X-ray transition radiation from regular radiators, Nucl. Instrum. Methods Phys. Res., Sect. A **696**, 141 (2012).

[30] J. Allison, K. Amako, J. Apostolakis *et al.*, Recent developments in GEANT4, Nucl. Instrum. Methods Phys. Res., Sect. A **835**, 186 (2016).

[31] G. M. Garibian, Radiation from a charged particle traversing a layered medium, J. Exp. Theor. Phys. **8**, 1003 (1959) [, Zh. Eksp. Teor. Fiz. **35**, 1435 (1959).

[32] G. M. Garibyan, L. A. Gevorgyan, and C. Yang, X-ray transition radiation produced in an irregular medium, J. Exp. Theor. Phys. **66**, 552 (1974).

[33] G. M. Garibian and Y. Shi, *X-Ray Transition Radiation* (Nauka Erevan, Russia, 1983).

[34] V. E. Pafomov, Radiation of a charged particle in the presence of a separating boundary, Trudy Fiz. Inst. im. P. N. Lebedeva, Ross. Akad. Nauk. **44**, 28 (1969).

[35] V. E. Pafomov, On the interference effects of radiation in layered media, Zh. Tekh. Fiz. **33**, 557 (1963) [Sov. Phys. Tech. Phys. **8**, 412 (1963)].

[36] V. E. Pafomov, Radiation of a charged particle in the presence of a separating boundary, *Nuclear Physics and Interaction of Particles with Matter*, edited by D. V. Skobel'tsyn, The Lebedev Physics Institute Series (Springer, Boston, MA, 1971), p. 25, Vol. 44.

[37] J. H. Hubbell and S. M. Seltzer, Tables of x-ray mass attenuation coefficients and mass energy-absorption coefficients 1 keV to 20 MeV for elements Z = 1 to 92 and 48 additional substances of dosimetric interest, NIST Interagency/Internal Report No. NISTIR5632, 2017.

[38] V. A. Bazylev, V. I. Glebov, E. I. Denisov, N. K. Zhevago, M. A. Kumakhov, A. S. Khlebnikov, and V. G. Tsinoev, X-ray Cerenkov radiation. Theory and experiment, J. Exp. Theor. Phys. **54**, 884 (1981).

[39] V. G. Baryshevsky, I. D. Feranchuk, and A. P. Ulyanenkov, Parametric x-ray radiation: Theory, experiment and applications, *Springer Tracts in Modern Physics* (Springer, Berlin, 2006), Vol. 213.

[40] H. Berger, Complex Doppler effect in dispersive media, Am. J. Phys. **44**, 851 (1976).

[41] D. Zeppenfeld, Collider Physics, *The proceedings of TASI-98, Neutrinos in Physics and Astrophysics*, edited by P. Langacker (World Scientific, Singapore, 2000), pp. 303–350.

[42] P. Goedtkindt, J.-M. Salomé, X. Artru, P. Dhez, M. Jablonka, N. Maene, F. Poortmans, and L. Wartski, Interference effects in X-ray transition radiation with a 500 MeV electron beam, Nucl. Instrum. Methods Phys. Res., Sect. B **56**, 1060 (1991).

[43] A. P. Potylitsyn, M. I. Ryazanov, M. N. Strikhanov, and A. A. Tishchenko, Diffraction radiation from relativistic particles, *Springer Tracts in Modern Physics* (Springer, Berlin, 2011), Vol. 239.